A Coupled DEM/CFD Analysis of the Effect of Air on Powder Flow During Die Filling

Y. Guo, K. D. Kafui, C.-Y. Wu, and C. Thornton
School of Chemical Engineering, University of Birmingham, Edgbaston, Birmingham, B15 2TT, U.K.

J. P. K. Seville
School of Engineering, University of Warwick, Coventry, CV4 7AL, U.K.

DOI 10.1002/aic.11734
Published online December 4, 2008 in Wiley InterScience (www.interscience.wiley.com).

Die filling from a stationary shoe in a vacuum and in the presence of air was numerically analyzed using an Eulerian-Lagrangian model, which employs a discrete element method (DEM) for the particles and computational fluid dynamics (CFD) for the air with a two-way air-particle interaction coupling term. Monodisperse and polydisperse powder systems have been simulated to explore the effect of the presence of air on the die filling process. For die filling with monodisperse powders, the influences of particle size and density on the flow behavior were explored. The numerical simulations revealed that the presence of air has a significant impact on the powder flow behavior, especially for systems with smaller and/or lighter particles. Flow has been characterized in terms of a dimensionless mass flow rate, and it has been shown that for die filling in a vacuum this is constant. The flow characteristics for die filling in air can be classified into two regimes. There is an air-inert regime in which the particle size and density are sufficiently large that the effect of air flow becomes negligible, and the dimensionless mass flow rate is essentially identical to that obtained for die filling in a vacuum. There is also an air-sensitive regime, for smaller particle sizes and lower particle densities, in which the dimensionless mass flow rate increases as the particle size and density increase. The effects of particle-size distribution and adhesion on the flow behavior have also been investigated. It was found that, in a vacuum, the dimensionless mass flow rate for polydisperse systems is nearly identical to that for monodisperse systems. In the presence of air, a lower dimensionless mass flow rate is obtained for polydisperse systems compared to monodisperse systems, demonstrating that air effects become more significant. Furthermore, it has been shown that, as expected, the dimensionless mass flow rate decreases as the surface energy increases (i.e., for more cohesive powders). © 2008 American Institute of Chemical Engineers *AIChE J,* 55: 49–62, 2009
Keywords: die filling, DEM, CFD, air effect, powder compaction, mass flow rate, adhesion

Introduction

Die filling is an important stage in powder compaction which is widely used in the powder metallurgy, ceramic, pharmaceutical and chemical industries. Powder flow during die filling is a key determinant of the outcome of the entire

Correspondence concerning this article should be addressed to C.-Y. Wu at c.y.wu@bham.ac.uk.

powder compaction process, and, therefore, exerts a significant influence on the final properties of the products.[1] Furthermore, a high powder flow rate and low segregation tendency during die filling are likely to improve the manufacturing efficiency and product quality. This has motivated increased interest in the study of powder flow characteristics during die filling.[2,3]

The flow behavior of powders during die filling is determined by a number of factors, including powder characteristics (particle size, size distribution, particle shape, density, initial packing or surface properties), apparatus features (shoe or die design), and operating conditions (speed, aeration, moisture, temperature, the presence of air, suction or history of applied stress). Many experiments have been conducted to evaluate the influence of these factors. Bocchini[4] observed that filling densities decrease with decreasing die width due to the presence of sparse boundary layers at the die walls. Haskins and Jandeska[5] used computed tomography to determine the spatial powder distribution, and found that the powder density distribution depends on the orientation of the die cavity and the die geometry. Demetry et al.[6] developed tactile sensors as a tool to evaluate the density uniformity in powder beds after die filling, and found that pouring the powder immediately above the die opening rather than from the side of the die results in a more uniform density distribution. The effects of several operating conditions such as shaking, settling time, the powder level in the shoe, and the presence of air on the die filling process have been examined by Sawayama and Seki.[7] They observed that the die filling speed can be increased by reducing the powder level in the shoe, shaking the shoe or using an air-replacement shoe. Hjortsberg and Bergquist[8] investigated the effects of shoe motion and powder level in the shoe on the density variation in a ring shaped die, and found that the powder density is higher in the sections orthogonal to the direction of shoe motion and increases with the settling time, shoe speed and number of shoe passages. However, the density was found to be insensitive to the amount of powder in the shoe if the powder level is above a critical value. Some other operating conditions, such as aeration or suction, were also found to have a significant impact on the filling process. It has been reported that the powder flow rate and uniformity of fill can be improved by using a fluidized fill shoe,[9] or a suction filling system.[10]

Using high-speed video observation of a model shoe-die filling rig, Wu et al.[11] investigated the influences of powder characteristics, shoe kinematics and air flow on the die filling process, and identified two powder flow patterns: nose flow, in which the powder flows over the surface of a nose shaped flow stream and avalanches into the die, and bulk flow, in which the powder is delivered into the die by detaching from the bottom surface of the powder mass. They found that the nose flow promotes fast-air evacuation and rapid free surface flow, so that the overall powder flow rate is increased when the nose flow becomes the dominant flow mechanism. When the die opening is completely covered by the powder, bulk flow starts to dominate the die filling process, the filling efficiency is decreased, and air flow becomes significant and inhibits the powder flowing into the die. For some pharmaceutical powders, Sinka et al.[12] and Schneider et al.[13] proposed a third flow mechanism: intermittent flow, in which the powder flow occurs as a result of a series of discrete instabilities with the release of large chunks of agglomerated powder into the die. In order to interpret the experimental results quantitatively, Schneider et al.[14] used dimensional analysis to provide a framework for extrapolating the results to other die and shoe geometries.

Die filling has also been modeled using DEM by Wu et al.[15] who demonstrated that DEM can model the powder flow behavior during die filling in a vacuum. A simplified algorithm was also incorporated in DEM by Wu and Cocks[16] to model the effect of the build-up of air pressure for die filling in air, where the air drag effect and particle-air interaction coupling effect were ignored. Although the study revealed that the simplified model can capture the essential feature of the build-up of air pressure on the flow kinematics of powder, they envisaged that there was still a need to develop a more rigorous model in which the dynamics of air and powder, and their interactions are considered thoroughly in order to model the major effects of air during die filling as observed experimentally.

Consequently, in this article, a coupled DEM and CFD method, in which the air-particle interaction is determined by a combination of pressure gradient, viscous stress and drag force, is employed to analyze the die filling process. This coupled DEM/CFD method has proved to be capable of modeling the complicated interaction between the air and the particles during fluidisation[17,18] and die filling.[19] Using the coupled DEM/CFD method, the effect of air on powder flow behavior during die filling is examined from simulations in air and in a vacuum. In addition, the influence of powder characteristics (particle size, density and size distribution) is investigated. Since most real powders, in particular, pharmaceutical powders, are more or less cohesive, simulations using cohesive powders are also performed to explore the influence of cohesion.

Computational Model

The coupled DEM/CFD method used in this study was originally developed by Kafui et al.[17] to model two-phase (gas-solid and liquid-solid) systems. The DEM/CFD code is an advanced version of TRUBAL, which is the DEM code originally developed by Cundall.[20] Using this method, a powder is modeled as an assembly of spherical solid particles which interact with each other, and the interactions are governed by rigorous contact models based on classical contact mechanics.[21–27] The position of each particle within the system is incremented at fixed time steps by integrating the equations of motion which are governed by Newton's second law. The air is treated as a continuous fluid phase governed by the continuity and momentum equations. A fluid-particle interaction scheme is introduced to model the two-way coupling between the two phases. A detailed description of the DEM/CFD method was provided by Kafui et al.,[17] and the distinctive features of the model used in this study are:

1. The interaction between elastic spheres is modeled using algorithms based on classical contact mechanics,[26] in which the theory of Hertz[21] is used to model the normal interaction, and the theory of Mindlin and Deresiewicz[28] is used for the tangential interaction. This enables the evolution of contacts to be determined using physically realistic parti-

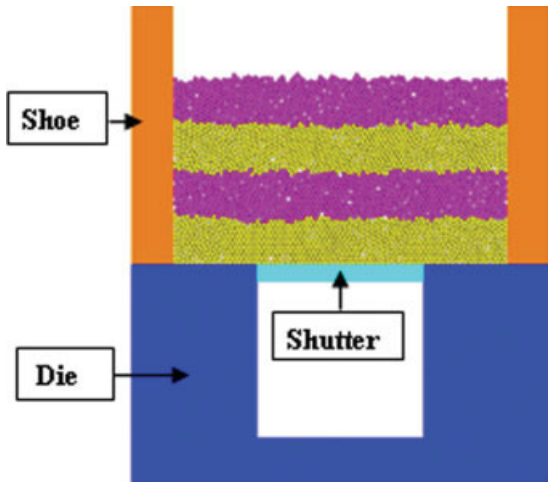

Figure 1. The numerical model for die filling.

[Color figure can be viewed in the online issue, which is available at www.interscience.wiley.com.]

cle properties, such as Young's modulus and Poisson's ratio, compared to many other DEM codes with spring-dashpot type contact models, in which artificial contact stiffness's are used, and the link with the physical properties of the particles is obscure.

2. Contact laws for autoadhesive particles have been developed and implemented so that cohesive powders can be modeled. The JKR theory,[22] which extends the Hertz theory to account for surface energy, is used to model the normal interaction, with the tangential interaction between autoadhesive particles modeled using the theory developed by Thornton.[23] Two-phase flow of autoadhesive particles in air can, therefore, be analyzed rigorously, enabling the flow and mechanics of cohesive powders in air and in a vacuum to be explored.

The Numerical Model of Die Filling

All simulations were performed in two dimensions, but the powder bed was treated as a monolayer of spheres, from which the void fraction is calculated with the average diameter as the thickness of the powder bed.[17] The schematic layout of the die filling system is shown in Figure 1. The system is composed of a top container, which is generally referred to as a shoe, a bottom container which is the die, and a shutter. Initially, a specified number of particles were randomly generated in the shoe, then deposited under gravity in the absence of air until they settled to a steady state with negligible kinetic energy, i.e., when the mean-particle velocity is of the order of 10^{-6} m/s or smaller. The powder bed is then color-banded so that the macroscopic flow patterns can be visualized. To consider the effect of air on the powder flow, air initially fills the void spaces in the shoe and die regions at uniform pressure (no pressure gradients). The computational fluid cells and boundary conditions used for the die filling simulations are schematically shown in Figure 2, in which the fluid region is partitioned uniformly. The air is modeled with interior fluid cells (1), the walls are treated as impermeable with no slip boundaries (3), and the top of the shoe is modeled using continuous gas outflow wall cells with free slip boundaries (6). All quantities such as air pressure and air velocity are averaged in the fluid cells, and the void fraction of each cell is defined by the total volume of particles inside the cell. As argued by Tsuji et al.[29] the size of the fluid cells should be smaller than the macroscopic motion of bubbles (to simulate the evolution of bubbles and the detailed fluid flow inside the bubbles), but larger than the particle size (to avoid zero void fractions). As typically adopted in simulations of fluidized beds,[29] the size of the fluid cells is set in the range of 3–5 times the average particle diameter in this study. The die filling process is started by suddenly removing the shutter so that the particles start to flow into the die under the influence of gravity.

In this study, except when stated otherwise, the particles are assumed to be elastic with a Young's modulus of 8.7GPa and Poisson's ratio of 0.3. The interparticle and particle-wall friction coefficients are set to a value of 0.3. The air has a temperature of 293 K and a viscosity of 1.8E-5 kg m^{-1} s^{-1}. Standard atmospheric pressure (101325 Pa) is assigned as the initial air pressure. For all simulations performed, the width of the shoe is set as twice that of the die.

Die fillings with monodisperse powders are considered first. Four groups of simulations have been performed to investigate the effects of particle size and density, as shown in Table 1. In Group 1, the solid particle density ρ_s is fixed at a value of 1,500 kg/m^3, and different particle sizes d_p are used to investigate the effect of particle size. In Group 2, the particle size is fixed at 130 μm, and different solid densities are used to investigate the effect of particle density. In Group 3, powders with particle sizes equal to or larger than 500 μm are used, and a larger die is used to maintain the ratio of particle size to the width of die opening. In Group 4, powders with a relatively large particle size of 340 μm and higher solid densities are used. Groups 3 and 4 are special cases with larger particle sizes and densities, for which the influence of air on the flow behavior is expected to be negligible. The reason to consider these two groups will be further dis-

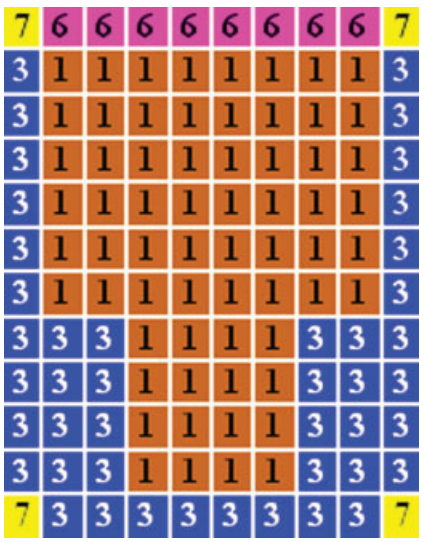

Figure 2. A schematic diagram of the computational fluid cells and boundary conditions.

[Color figure can be viewed in the online issue, which is available at www.interscience.wiley.com.]

Table 1. Simulation Groups

	Die size (mm)	Particle diameter d_p (μm)	Solid density ρ_s (kg/m^3)	Void fraction ε
Group 1	2×2	25	1500	0.448
		40		0.450
		50		0.447
		60		0.449
	7×7	90	1500	0.447
		130		0.450
		180		0.449
		260		0.453
		340		0.447
		430		0.457
Group 2	7×7	130	400	0.447
			700	0.451
			1500	0.450
			2500	0.449
			3500	0.448
			5500	0.449
			7800	0.450
Group 3	18×18	500	1500	0.448
		600		0.447
		700		0.448
		800		0.448
		900		0.449
Group 4	7×7	340	3000	0.447
			5000	0.448
			7000	0.447

cussed in the next section. After initial deposition, all the powder beds considered have similar void fractions in the range of 0.447–0.457.

Die Filling with Monodisperse Powders

Die filling in air and in a vacuum

The presence of air can have a significant impact on the flow behavior of powders during die filling.[11,16] In order to compare the flow behavior of powder during die filling in air and in a vacuum, simulations with a monodisperse powder system composed of particles of diameter 50 μm and density 1,500 kg/m^3 were performed. Figure 3 shows the time history of the mass of particles fed into the die for die filling in a vacuum and in air. It is found that for die filling in a vacuum the flow of powder into a die is accelerated from the initial steady state. A relatively low mass flow rate is observed at the very early stage of the process immediately after the shutter is removed (say $t < 0.005$ s). The flow rate increases very sharply thereafter, and remains constant during most of the filling process until the die is almost completely filled when a deceleration stage is then observed. For die filling in air, it is also observed that there is an acceleration stage at the beginning of die filling, and a deceleration stage when the die is almost completely filled. However, the powder flow process in air can be divided into two distinct regimes: a slow flow regime at the early stage of die filling up to the instant A3 (as labeled in Figure 3), and a fast flow regime thereafter. It is evident that the die is filled much more slowly in air than in a vacuum. This is due to the counter-flow of the air against the direction of the powder flow. In order to explore the mass flow behavior presented in Figure 3, a detailed examination of the flow patterns of powder and air was carried out and the results are presented in Figures 4–8, in which typical features are shown at various instants labeled in Figure 3.

Figure 4 shows the powder flow patterns for die filling in a vacuum. It can be seen that the powder flows into the die smoothly and quickly with two narrow regions of retarded flow adjacent to the edge of the die opening, forming two narrow empty regions close to the die walls. This pattern is consistent with the experimental observation of powder discharge from a bin and is generally referred to as the empty annulus.[30] The contact force distributions for the powder at various instants are shown in Figure 5, in which the lines are drawn passing through the contact points in the direction of the forces, with the thickness of the lines indicating the magnitude of the local contact force relative to the current maximum contact force. It is observed that as the powder flow into the die commences, the contact forces disappear quickly from the bottom of the powder bed over the die opening (Figure 5b–e). This absence of any significant number of interparticle contact forces persists until the die is almost completely filled, whereupon a dense enduring contact force network is formed (Figure 5f).

The powder flow behavior during die filling in air is shown in Figure 6, and the corresponding contact force distributions and air velocity and pressure distributions are given in Figures 7 and 8, respectively. In Figure 8, the length of the vectors represents the relative magnitude of the local air velocity scaled to the maximum air velocity during the whole die filling process. It can be seen that due to the presence of air in the die, the powder initially flows into the die very slowly and mainly from the center of the die opening (Figure 6a,b). Thus, two air bubbles are formed next to the die walls and separated by the flowing powder at the center (Figure 6b). The contact force network above the die opening persists over an extended period of time compared to that in a vacuum (Figure 7a–c). The air is initially dragged by the flowing powder to flow downward at the center of the die. Due to the restriction of the die boundaries, the air flows

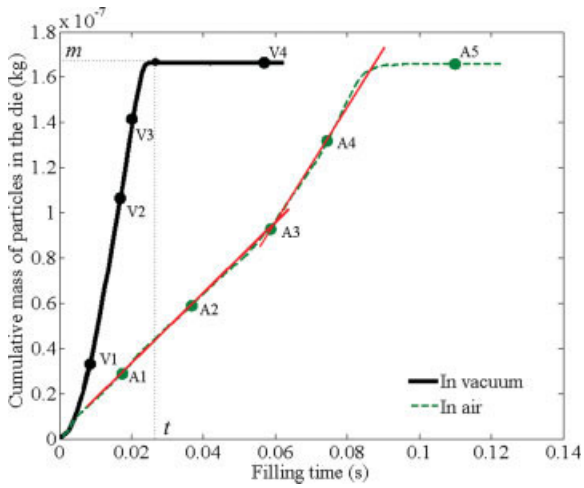

Figure 3. The variation of the mass of particle deposited into the die with the filling time for die filling in a vacuum and in air.

(Die size: 2 mm × 2 mm). [Color figure can be viewed in the online issue, which is available at www.interscience.wiley.com.]

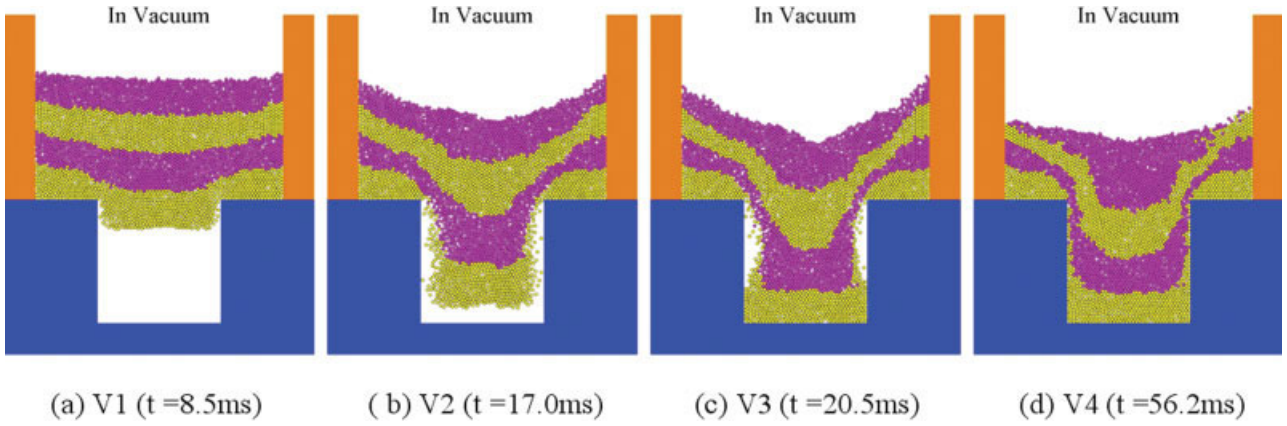

Figure 4. Powder flow behavior during die filling in a vacuum.

[Color figure can be viewed in the online issue, which is available at www.interscience.wiley.com.]

sideways at the bottom and then turns upward (Figure 8a). As shown in Figure 8b, the air flows upward at a higher velocity in the centers of the bubbles, and it is also observed that the air, dragged by downward flowing clusters of particles along the die walls (Figure 6b), flows downward near the die walls. As the powder flows into the die, the volume of the free space occupied by air decreases, and, therefore, the overall pressure of the entrapped air increases (Figure 8a,b). The pressure distribution with a striped pattern is observed in Figure 8b. This striped pattern is formed as a result of the air being compressed by the main powder stream flowing in the center with clusters of particles falling

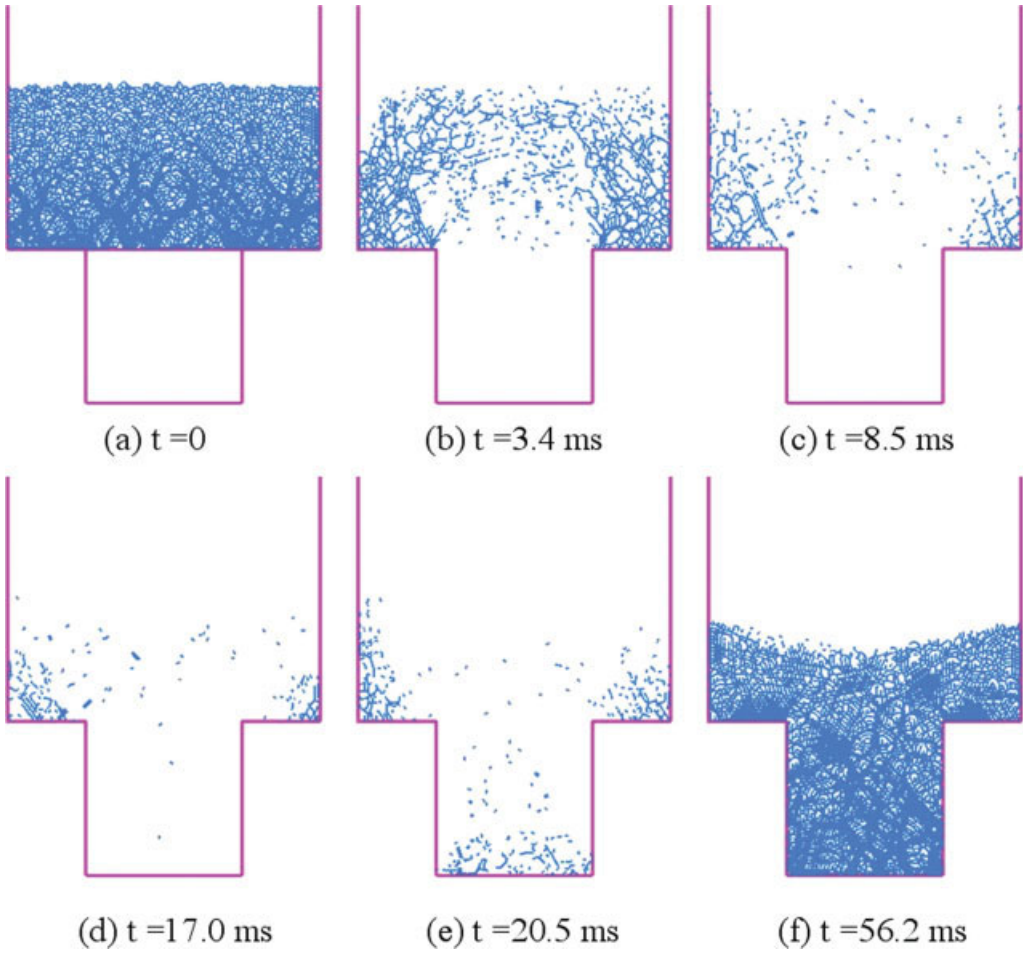

Figure 5. Contact force distributions during die filling in a vacuum.

[Color figure can be viewed in the online issue, which is available at www.interscience.wiley.com.].

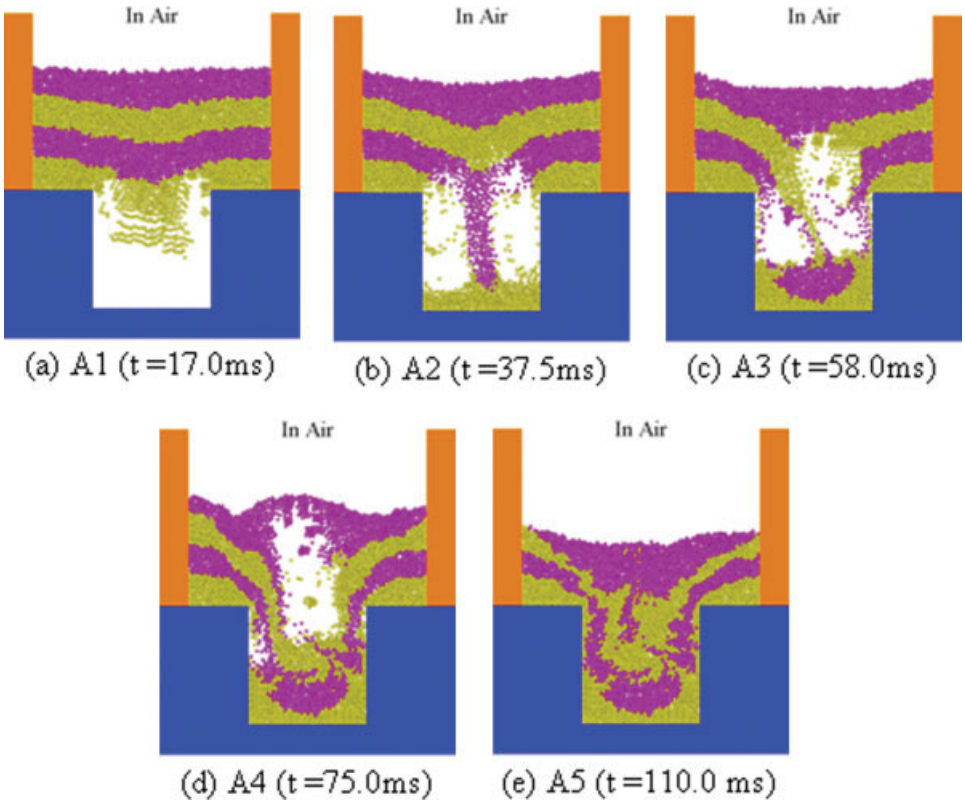

Figure 6. Powder flow behavior during die filling in air.

[Color figure can be viewed in the online issue, which is available at www.interscience.wiley.com.]

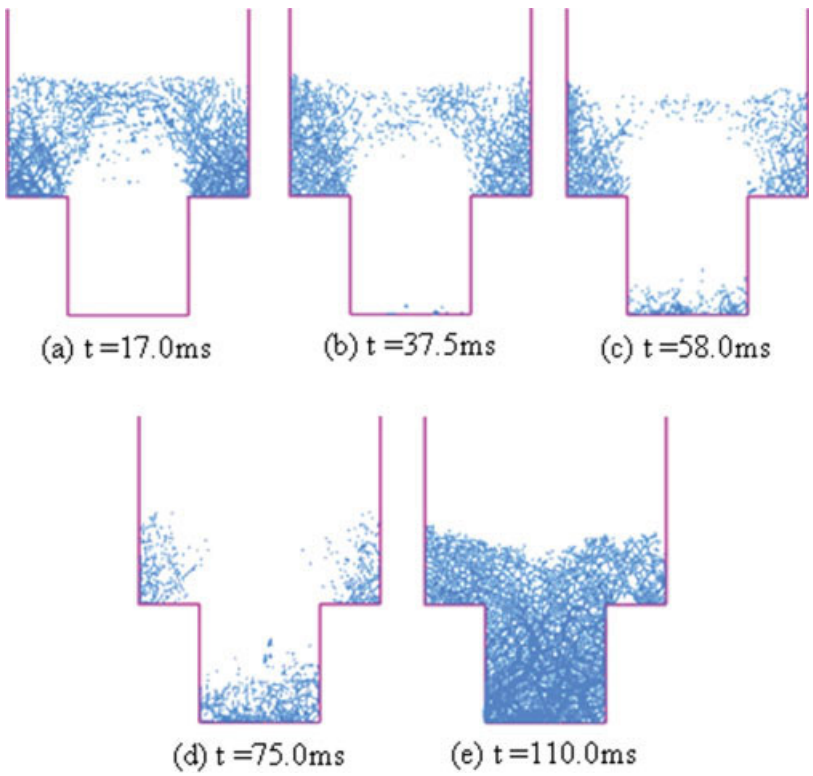

Figure 7. Contact force distributions during die filling in air.

[Color figure can be viewed in the online issue, which is available at www.interscience.wiley.com.]

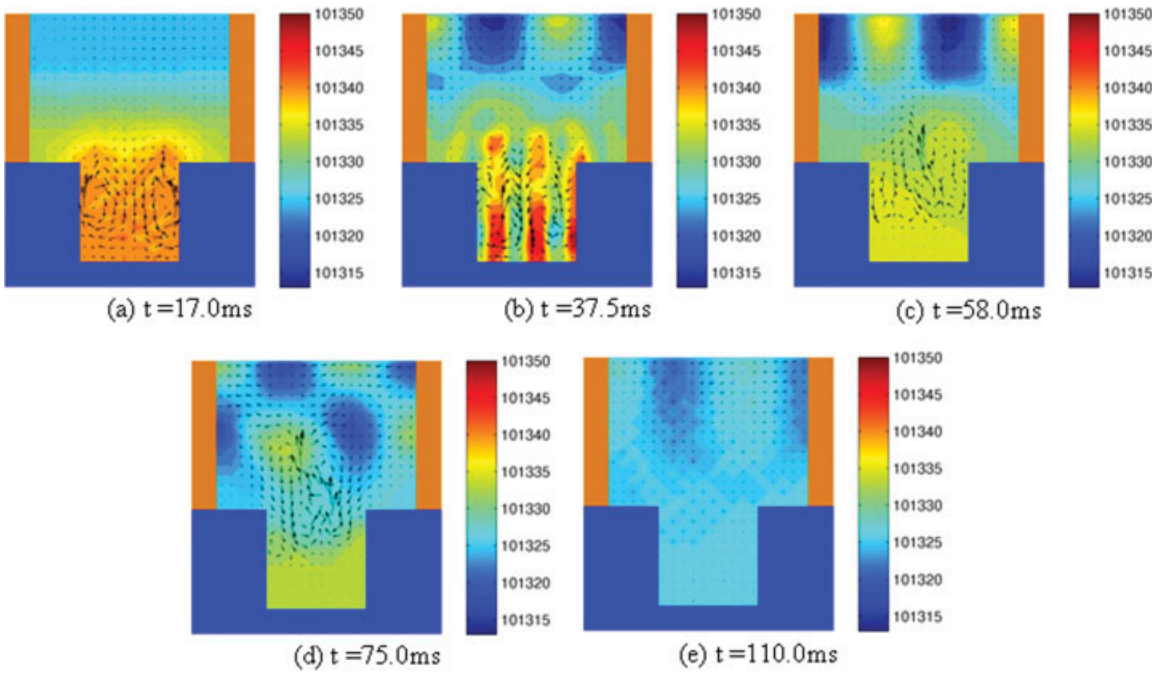

Figure 8. Air velocity and pressure distributions during die filling in air.

[Color figure can be viewed in the online issue, which is available at www.interscience.wiley.com.]

close to the die walls. Consequently, low-pressure bands are created along the flow paths of the main powder stream, and the clusters of particles and high-pressure bands are induced between. The filling process, hence, becomes much less steady and the entrapped air bubbles hinder and disturb the powder flow, which induces a slow powder flow as observed in Figure 3. As more powder flows into the die, the bubbles rise. One of them gradually shrinks and disappears, whereas the other one grows and continues to rise until it erupts at the top surface of the powder bed (Figures 6c,d). It is interesting to note that once the center of the larger entrapped bubble reaches the top of the die (Figure 6c), the powder flows easily into the die from the sides of the larger bubble. As a result, the mass flow rate is increased after the instant A3 shown in Figure 3. With the larger bubble moving out of the die, the contact force network above the die opening gradually disappears (Figures 7c,d). As the air permeates through the expanded loose powder layers above the die opening, the air pressure inside the bubbles decreases (Figures 8c,d). The strong interaction between the powder and the entrapped air leads to a significant mixing of particles when they are deposited into the die (Figure 6e). Once the die filling process is completed, an enduring contact force network is re-established (Figure 7e). Simultaneously, the air velocity decelerates to zero and the air pressure in the pores of the deposited powder reverts to the atmosphere pressure (Figure 8e).

Mass flow rate during die filling

In order to quantify the powder flow during die filling, an average mass flow rate $\overline{M}$ is defined as

$$\overline{M} = \frac{m}{t}. \tag{1}$$

in which m is the total mass of particles deposited in a fully-filled die, t is the duration of die filling, and is the time when the die is just completely filled (see Figure 3). For the die filling cases considered in Figure 3, the average mass flow rate in air ($\overline{M} = 1.71 \times 10^{-6}$ kg/s) is much lower than that in a vacuum ($\overline{M} = 6.51 \times 10^{-6}$ kg/s).

The process of powder flow from a stationary shoe is somewhat analogous to hopper flow and the flow of a powder from a bin, for which Beverloo et al.[31] proposed a well-known empirical equation for the solid discharge rate from a circular orifice in the form

$$M = C\rho_b g^{1/2} {D_0}^{5/2} \left(1 - k\frac{d_p}{D_0}\right)^{5/2} \tag{2}$$

in which M is the mass flow rate, C is a dimensionless constant, ρ_b is the bulk density of the powder, g is the acceleration due to gravity, D_0 is the diameter of the circular orifice, d_p is the mean-particle diameter, k is a constant that is found to depend only on the particle shape having a value of about 1.5 for spherical particles.[30] Note that $[1 - k(d_p/D_0)]$ is a correction for the orifice size due to the presence of an "empty annulus", which is a region of retarded flow adjacent to the orifice edge (see also Figure 4).

Theoretical models have also been proposed to predict the discharge rates of granular materials from storage bins or hoppers. Many of these models are based on the concept of the "free-fall arch", which is an arch located at the lower boundary surface of the powder bed. Above the free-fall arch, particles are in contact with each other. Below the arch, particles are no longer in contact and freely accelerate under gravity. Based on experimental observations, Harmens[32] assumed that the powder flow from a container is

independent of the bed depth H, and the shape of the free-fall arch is independent of the scale, so that the arch height above the circular orifice is of the order of the diameter D_0. When the particles are accelerating freely under gravity after detaching from the arch, their velocities on passing through the orifice are of the order of $(gD_0)^{1/2}$. By considering the cross-sectional area of the orifice $\pi D_0^2/4$, the flow rate is thus proportional to $g^{1/2}{D_0}^{5/2}$, which is the same dependence as in Eq. 2. If the thickness of the container is far smaller than the width of the orifice, the powder flow can be treated as a quasi-two-dimensional (2-D) planar flow. The shape of the orifice is then a narrow rectangle of dimensions $b_0 \times l$, where b_0 is the width of the orifice, and l is the thickness of the container. Under this condition, by a similar analysis to the aforementioned, the height of the free-fall arch is shown to be of the order b_0. Thus, the particle velocity passing through the orifice is of the order $(gb_0)^{1/2}$. Considering the sectional area $b_0 l$, the flow rate is proportional to $g^{1/2} l b_0^{3/2}$.

Brown and Richards[33] developed a "minimum energy theorem" to describe powder flow with a spherical free-fall arch. They obtained a volumetric flow rate equation for the powder discharge from a circular orifice in the form

$$M_v = \frac{\sqrt{2\pi}}{6} g^{1/2} D_0^{5/2} (1 - \cos^{3/2}\beta) \big/ \sin^{5/2}\beta \tag{3}$$

in which M_v represents volumetric flow rate, and β is the half-angle of the flowing zone. It can be seen that the flow rate is proportional to $g^{1/2}D_0^{5/2}$, which is consistent with the Beverloo equation (Eq. 2), regardless of the effect of the "empty annulus". Based on this theory, a volumetric flow rate for planar flow can also be derived. As indicated by Brown and Richards,[33] the radial velocity in plane strain is given by

$$v_r = \frac{g^{1/2} r_0^{3/2} \cos^{1/2}\theta}{r} \tag{4}$$

where r_0 is the radius of curvature of the free-fall arch, r and θ are the radial and angular coordinates, respectively, for a position in the flowing zone. Thus, the volumetric flow rate for planar flow can be written as

$$M_v = 2\int_0^\beta v_r \, l r \, \mathrm{d}\theta = 2 g^{1/2} \, l \, r_0^{3/2} \int_0^\beta \cos^{1/2}\theta \, \mathrm{d}\, \theta \tag{5}$$

where l is the thickness of the powder bed. Since the width of the orifice $b_0 = 2r_0 \sin\beta$

$$M_v = \frac{\sqrt{2}}{2} g^{1/2} l \, b_0^{3/2} \frac{\int_0^\beta \cos^{1/2}\theta \, \mathrm{d}\theta}{\sin^{3/2}\beta} \tag{6}$$

Davidson and Nedderman[34] proposed a mass flow rate equation for quasi-two-dimensional hopper flow as

$$M = \frac{\rho_b g^{1/2} l b_0^{3/2}}{\sin^{1/2}\alpha} \left[\frac{1+K}{2(K-2)}\right]^{1/2} \tag{7}$$

in which b_0 is the orifice width, l is the hopper thickness, α is the hopper half-angle, K is a function of the internal friction angle and is in the range of 2.5–7.5 for commonly encountered materials.[30]

The above analyses independently demonstrate that the flow rate is proportional to $g^{1/2} l b_0^{3/2}$ for the quasi-two-dimensional planar flow. Hence, a dimensionless flow rate M^* is proposed as

$$M^* = \frac{\overline{M}}{\rho_b g^{1/2} l {b_0}^{3/2} \left(1 - k\frac{d_p}{b_0}\right)^{3/2}} \tag{8}$$

where $\overline{M}$ is the average mass flow rate defined in Eq. 1. In Eq. 8, the presence of the retarded flow region adjacent to the orifice edge (empty annulus) is also considered, so $[1 - k(d_p/b_0)]$ is a correction for the die opening size. Schneider et al.[14] indicated that under conditions where core flow occurs in a vacuum, M^* depends only on particle-particle and particle-wall frictions for a given shape of orifice, i.e.

$$M^* = f(\mu_p, \mu_{pw}). \tag{9}$$

where μ_p is the friction coefficient between particles, and μ_{pw} is the friction coefficient between a particle and a wall. For given materials (with load-independent friction coefficients) therefore, M^* is expected to be constant.

As the powder flows into a die in the presence of air, a negative pressure gradient is created that opposes the powder flow. The built-up air pressure in the closed die enhances this negative pressure gradient to further slow down the powder flow, as demonstrated in Figures 6–8. By decreasing the void fraction, the permeability of the bulk material is decreased, so that it is more difficult for the entrapped air to escape, and the powder flow is hindered further. The drag force exerted by the air on the particles is proportional to the square of the superficial relative velocity (relative velocity between the air and the particle), which is related to the width of die opening b_0, because both the air and particle velocities are functions of position which is scaled by b_0. The air drag also depends on the particle size d_p and air viscosity η. In addition, by increasing the solid density ρ_s, the ratio of the drag force to the inertia of particles is decreased so that the impact of air on particles is decreased. In summary, during die filling in the presence of air, the dimensional flow rate M^* can be influenced by a number of additional factors, including the particle size d_p (and shape), solid density ρ_s, air viscosity η, width of the die opening b_0, and void fraction ε.

Following Schneider et al.,[14] taking the bulk density $\rho_b = (1 - \varepsilon)\,\rho_s$, g and b_0 as the independent variables, the following two dimensionless groups are introduced

$$\eta^* = \frac{\eta}{\rho_b g^{1/2} b_0^{3/2}}, \tag{10}$$

and

$$d_p^* = \frac{d_p}{b_0}. \tag{11}$$

The dimensionless flow rate during die filling in air can then be written as

$$M^* = f(\eta^*, d_p^*, \varepsilon, \mu_p, \mu_{pw}, \text{ particle shape}). \tag{12}$$

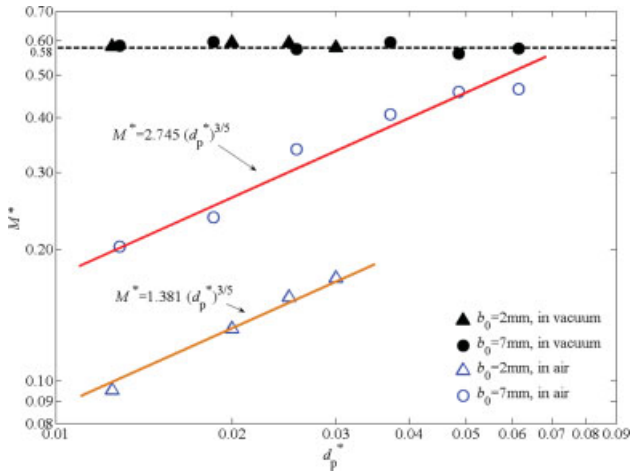

Figure 9. M^* vs. d_p^* for die filling in a vacuum and in air.

[Color figure can be viewed in the online issue, which is available at www.interscience.wiley.com.]

To a first approximation, the relationship between M^* and η^*, d_p^* is assumed to be a power law in the form of

$$M^* = A(\eta^*)^{-m}\left(d_p^*\right)^n. \tag{13}$$

where A, m and n are dimensionless parameters depending on void fraction ε, friction coefficients μ_p and μ_{pw}, and particle shape. These parameters can be determined by fitting the power-law relationship to the data over a range of values of η^* and d_p^*.

For die filling using monodisperse systems with a constant particle density and varying particle size (Group 1 in Table 1) the dimensionless flow rate M^* is plotted as a function of d_p^* in Figure 9. It can be seen that for die filling in a vacuum, the dimensionless flow rate M^* is essentially constant with an average value of 0.58. This is in excellent agreement with the Beverloo constant C determined experimentally,[30] which is reported to be in the range 0.55–0.65. For die filling in air, M^* increases with increasing size ratio d_p^* for a given die opening size b_0. This can be explained as follows. The air drag force on each particle is proportional to $C_D d_p^2$, where C_D is the particle drag coefficient, and the gravity force on the particle is proportional to d_p^3, so the ratio of drag force to gravity is proportional to $C_D(1/d_p)$. Considering that C_D decreases with increasing particle size d_p, the air drag effect becomes less significant as the particle size increases. As a result, the mass flow rate becomes higher with larger particles due to the reduced effect of air drag. It is interesting to note in Figure 9 that, on a log-log plot, the M^* vs. d_p^* curves for different die opening sizes are essentially straight lines and parallel to each other. The best fit curves reveal that M^* is proportional to $(d_p^*)^{3/5}$, i.e.

$$M^* = \xi\left(d_p^*\right)^{3/5} \tag{14}$$

where ξ is a parameter depending on the particle density and the die opening size.

From the results of the simulations using the parameters given for Group 2 in Table 1, M^* is plotted against η^* in Figure 10. It is clear that, for die filling in a vacuum, M^* is again constant at a value of 0.58. For die filling in air, M^* decreases as η^* increases. The relationship between M^* and η^* can be approximated as

$$M^* = 0.00272(\eta^*)^{-2/5}. \tag{15}$$

From Eqs. 10 and 15 with $\rho_b = (1 - \varepsilon)\,\rho_s$, we obtain

$$M^* \propto \rho_s^{2/5} \tag{16}$$

for die filling in air. This indicates that the dimensionless flow rate M^* in air increases with increasing solid density of the particles, due to the reduced effect of drag force relative to the inertia of particles.

From Eqs. 13, 14 and 15, we can write

$$M^* = A(\eta^*)^{-2/5}\left(d_p^*\right)^{3/5} \tag{17}$$

The dimensionless mass flow rates M^* for all the cases listed in Table 1 are plotted against $(\eta^*)^{-2/5}(d_p^*)^{3/5}$ in Figure 11. It is clear that the data coalesce onto two master curves for die filling in air and in a vacuum, respectively. For die filling in a vacuum, the dimensionless flow rate M^* is essentially constant at a value of 0.58, and is independent of particle size and particle density. This result is in excellent agreement with the previous studies of hopper flow and powder flow from bins,[30,31,35] in which the coarse powders were used and the effect of air could be neglected. For die filling in air, the results are distinguished by two regions. For high-values of $(\eta^*)^{-2/5}(d_p^*)^{3/5}$, M^* is essentially constant and close to the result obtained for die filling in a vacuum. For smaller values of $(\eta^*)^{-2/5}(d_p^*)^{3/5}$, M^* increases linearly with $(\eta^*)^{-2/5}(d_p^*)^{3/5}$, and the best fit to the data in this regime gives

$$M^* = 0.0296(\eta^*)^{-2/5}(d_p^*)^{3/5} \tag{18}$$

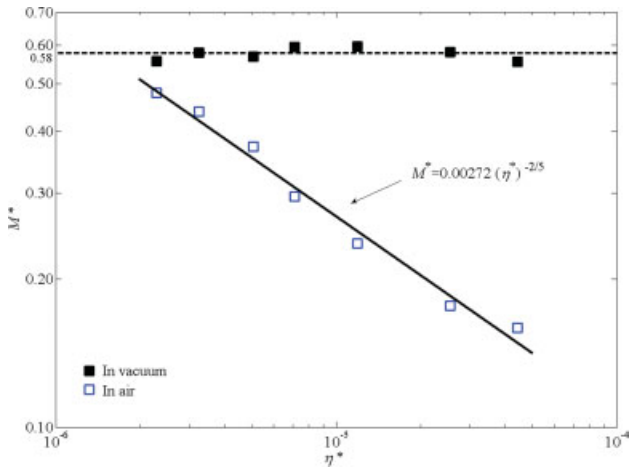

Figure 10. M^* vs. η^* in a vacuum and in air.

[Color figure can be viewed in the online issue, which is available at www.interscience.wiley.com.]

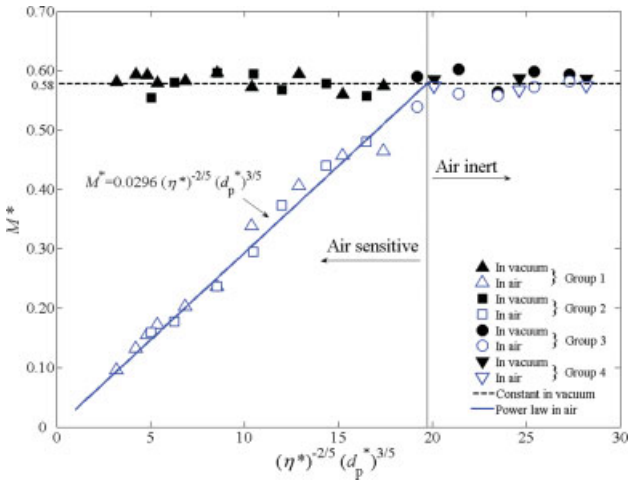

Figure 11. M^* vs. $(\eta^*)^{-2/5}\,(d_p^*)^{3/5}$ in a vacuum and in air.

[Color figure can be viewed in the online issue, which is available at www.interscience.wiley.com.]

The demarcation between these two regimes can be determined by setting $M^* = 0.58$ in Eq. 18. This leads to

$$(\eta^*)^{-2/5}(d_p^*)^{3/5} = 19.6 \tag{19}$$

Therefore, the intersection point $(\eta^*)^{-2/5}(d_p^*)^{3/5} = 19.6$ can be treated as a critical value to classify the two distinct regimes of flow behavior during die filling in air. If the value of $(\eta^*)^{-2/5}(d_p^*)^{3/5}$ is less than this critical value, which implies smaller or lighter particles, the powder flow rate is influenced and reduced significantly by the presence of air, and the flow rate is given by Eq. 18. This regime is referred to as the air-sensitive regime. If the value of $(\eta^*)^{-2/5}(d_p^*)^{3/5}$ is greater than the critical value, which implies larger or heavier particles, then the effect of air on the powder flow becomes negligible, and the flow rate in air is close to that in a vacuum. We refer to this regime as the air-inert regime. This distinction should be a useful guide for evaluating the influence of the presence of air on the powder flow behavior during die filling.

By substituting for η^* and d_p^* using Eqs. 10 and 11, Eq. 17 can be written as

$$M^* = B\left(\frac{\rho_s^2 g {d_p}^3}{\eta^2}\right)^{1/5} \tag{20}$$

where $B = A(1-\varepsilon)^{2/3}$. Considering the particle solid density ρ_s is generally much greater than the air density ρ_s (1.2 kg/m^3), the Archimedes number for the particles flowing in air can be written as[30]

$$\mathrm{Ar} = \frac{\rho_a(\rho_s-\rho_a)g d_p^3}{\eta^2} \approx \frac{\rho_a\rho_s g d_p^3}{\eta^2} \tag{21}$$

From Eqs. 20 and 21, the dimensionless mass flow rate M^* can be rewritten in terms of the Archimedes number and particle-air density ratio as

$$M^* = B\left(\mathrm{Ar}\cdot\Phi_\rho\right)^{1/5} \tag{22}$$

where Φ_ρ represents particle-air density ratio (i.e., $\Phi_\rho = \rho_s/\rho_a$). A re-plot of Figure 11 is shown in Figure 12, in which M^* is plotted against $\mathrm{Ar}\cdot\Phi_\rho$. It is clear that two distinct regimes (i.e., air-sensitive and air-inert) can also be classified by a critical value of $\mathrm{Ar}\cdot\Phi_\rho = 9.56\times10^6$. The best fit to the data in the air-sensitive regime gives

$$M^* = 0.0233\left(\mathrm{Ar}\cdot\Phi_\rho\right)^{1/5} \tag{23}$$

as shown by the solid line in Figure 12.

Die Filling with Polydisperse Powders

In reality, monodisperse particle systems are rare. Most powders are polydisperse. Hence, die filling of polydisperse powders has also been investigated. Two groups of polydisperse powders were examined. For these two groups, normal (Gaussian) particle-size distributions were assumed with the average particle size set to 130 μm and 180 μm, respectively. For each group, nine different size fractions were considered. The particle-size distribution for the polydisperse system with an average particle diameter of 130 μm, and a particle size in the range 50–210 μm is shown in Figure 13. For the system with an average particle diameter of 180 μm, the range of particle sizes was 100–260 μm. After initial deposition in the shoe, the void fractions of the polydisperse powders with the average particle diameters of 130 μm and 180 μm were 0.382 and 0.415, respectively.

Figure 14a shows a comparison of mass flow between the polydisperse powder system and a corresponding monodisperse system, having the same average particle diameter of 130 μm. For die filling in a vacuum, the mass flow rate is higher for the polydisperse system. For die filling in air, the mass flow rate is slightly higher when a monodisperse system is used, rather than a polydisperse one. In addition, a larger mass of powder in a fully-filled die is obtained when the polydisperse system is used whether in a vacuum or in air, because of the effect of dispersion on final void fraction. To compensate for this, the volumetric flow is also presented

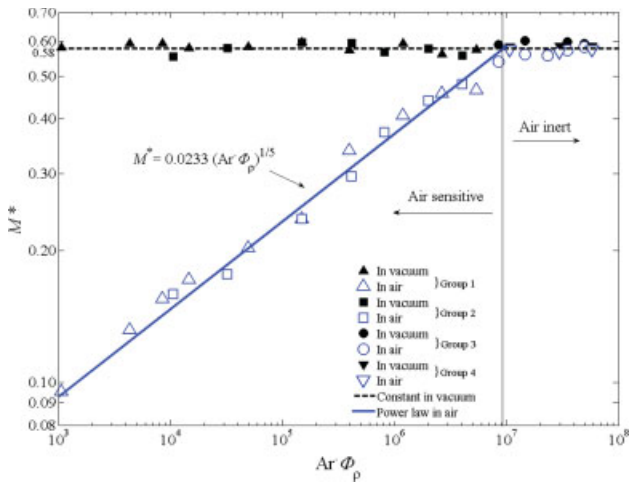

Figure 12. M^* vs. $\mathrm{Ar}\cdot\Phi_\rho$ in a vacuum and in air.

[Color figure can be viewed in the online issue, which is available at www.interscience.wiley.com.]

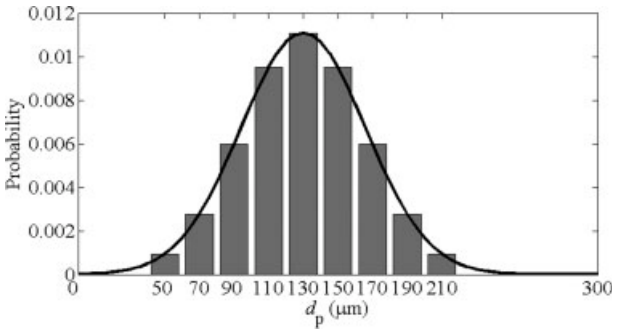

Figure 13. Typical particle-size distribution.

in Figure 14b, in which the apparent volume is defined as the mass divided by the initial bulk density. It is clear that, for die filling in a vacuum, the volumetric flow rates are the same for both polydisperse and monodisperse powders. For die filling in air, the volumetric flow rate is lower for the polydisperse powder compared to the monodisperse one. This implies, not surprisingly, that the influence of air becomes more significant when a polydisperse powder is considered. Similar trends were found for die filling with monodisperse and polydisperse powders with an average particle diameter of 180 μm. For powders with the same average particle diameter, the void fraction is lower for the polydisperse powder compared to the monodisperse powder. Therefore, during die filling with a polydisperse powder, the mass flow rate could be higher due to the denser packing regardless of the effect of air. However, the volumetric flow rate could be lower with a polydisperse powder in the presence of air, since the entrapped air in the die encounters a greater resistance in permeating the powder bed due to the lower void fraction, and a higher negative pressure gradient is generated to hinder the powder flow. Consequently, larger air bubbles are formed and a narrower flow stream is induced during die filling with polydisperse powders, as shown in Figure 15, which leads to a slower powder flow rate.

Figure 16 shows a comparison of the dimensionless mass flow rate M^* obtained for the monodisperse and polydisperse powder systems. By different random generations of particles, three simulations with different initial configurations of the powder bed in the shoe have been performed for each set of conditions. The bar graph shows the mean value of M^* for each set, with the error bar representing the standard deviation. It can be seen that, for die filling in a vacuum M^* is almost identical for all systems. For die filling in air M^* is reduced slightly for the polydisperse powders due to the lower void fraction.

Die Filling of Cohesive Powders

Most powders are to some extent cohesive, particularly in the case of powders with particle sizes less than 100 μm.[30] In order to study the effect of adhesion on powder flow during die filling, surface energy was introduced for the monodisperse powder with a particle diameter of 50 μm. In these simulations, the adhesive contacts for particle-particle and particle-wall are modeled according to the JKR theory.[22,23] The surface energy γ is prescribed by assuming the "pull-off" force is equal to k times the weight of a particle, i.e.

$$P_c = 3\pi\gamma R^* = k \cdot m_p g \tag{24}$$

so

$$\gamma = k \cdot \frac{m_p g}{3\pi R^*}. \tag{25}$$

Thus, different surface energies γ can be specified to obtain different values of k. In addition, noncohesive powder can be treated as a special case with k equal to zero.

Figure 17 shows the comparison of mass flow with and without adhesion. For the powder with adhesion, k is set to 4 (corresponding to $\gamma = 3.27 \times 10^{-5}$ J/m^2). It can be seen that for die filling in a vacuum, the flow of cohesive powder is slightly slower than that without adhesion, and slightly fewer

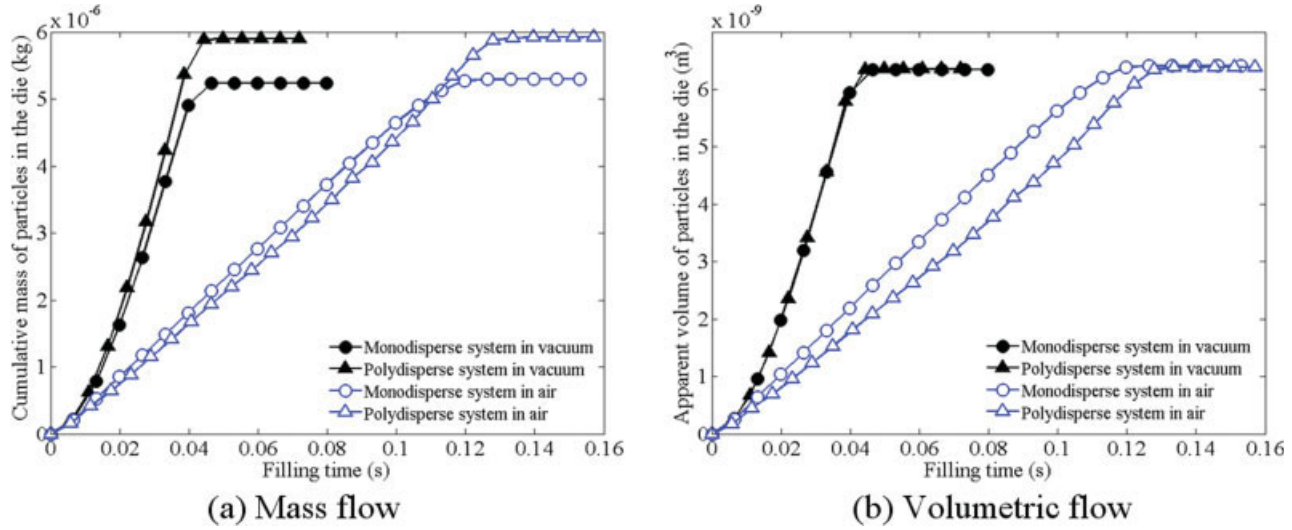

Figure 14. Mass flow (a) and volumetric flow, and (b) for monodisperse and polydisperse powder systems with average particle diameter of 130 μm.

(Die size: 7 mm × 7 mm). [Color figure can be viewed in the online issue, which is available at www.interscience.wiley.com.]

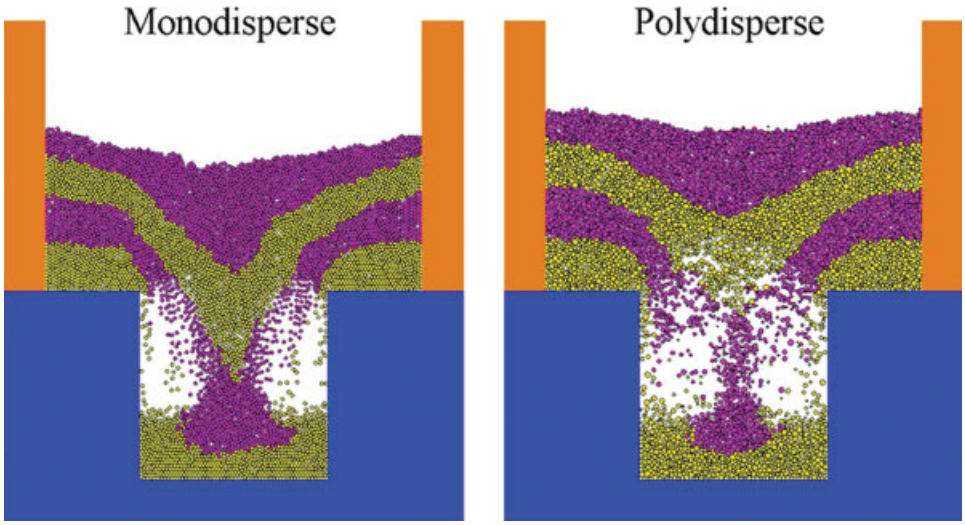

Figure 15. A comparison of powder flow patterns at the same moment in time during die filling for the monodisperse and polydisperse powder systems in the presence of air.

The two powders have the same average particle diameter of 130 μm. [Color figure can be viewed in the online issue, which is available at www.interscience.wiley.com.]

particles flow into the die. For die filling in air, the flow of the cohesive powder is clearly slower than that of a noncohesive powder, although the flow patterns are similar with a distinctive two-stage form. As expected, the powder flow in air is generally slower compared to the flow in a vacuum due to the effect of air. Figure 18 shows the powder flow pattern and contact force distribution in a vacuum at the same instant (t = 17.0 ms) as those shown in Figures 4b and 5d for die filling without adhesion. Compared to Figures 4b and 5d, it is clear that the die filling with a cohesive powder is slower than that for a noncohesive powder (Figure 18a), and the stagnant zones on the ledges of the die are larger for the cohesive powder (Figure 18b). The powder flow pattern and corresponding contact force distribution for die filling with a cohesive powder in the presence of air at the instant t = 75 ms are shown in Figure 19, which may be compared with Figures 6d and 7d. From the comparison, it is clear that for die filling with a cohesive powder in air, there are more particles still above the die opening at this instant (Figure 19a), and the contact force network can survive much longer when the particles are adhesive (Figure 19b). This is because of the adhesive particles sticking together, and, consequently, it becomes harder for the air flow to break the particle bonds and permeate the more constricted air pockets. As a result, the die is filled more slowly in the case of cohesive powders. The dimensionless mass flow rates for die fillings with and without adhesion in air and in a vacuum are compared in Figure 20. Again, each simulation was run in triplicate with different initial configurations of the powder bed in the shoe, and the mean value of M^*, and the error bar representing the standard deviation are presented in Figure 20. It is clear that for die filling with the cohesive powder, M^* is slightly lower

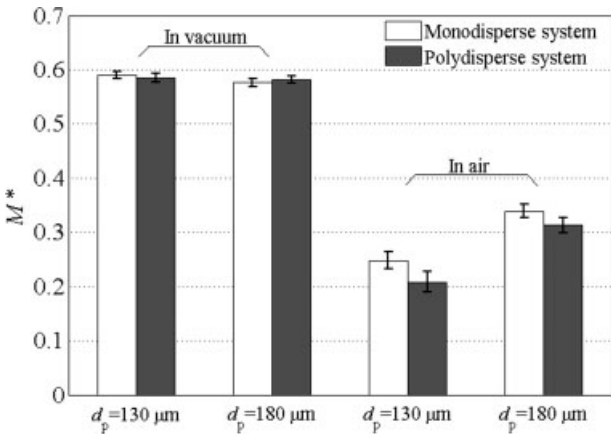

Figure 16. A comparison of dimensionless flow rates for monodisperse and polydisperse powder systems.

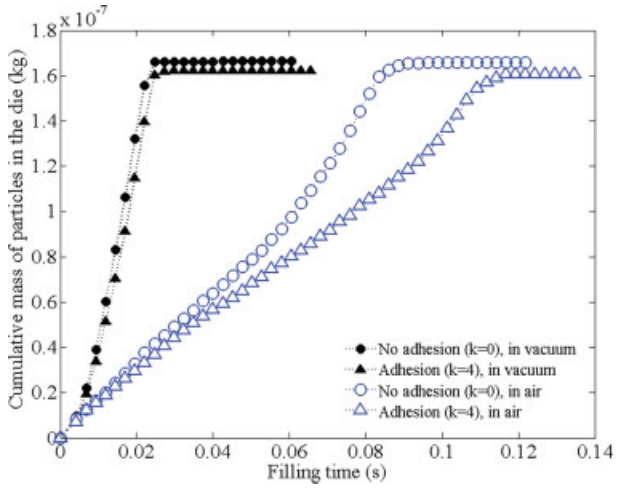

Figure 17. Mass flow with and without adhesion.

(Die size: 2 mm × 2 mm). [Color figure can be viewed in the online issue, which is available at www.interscience.wiley.com.]

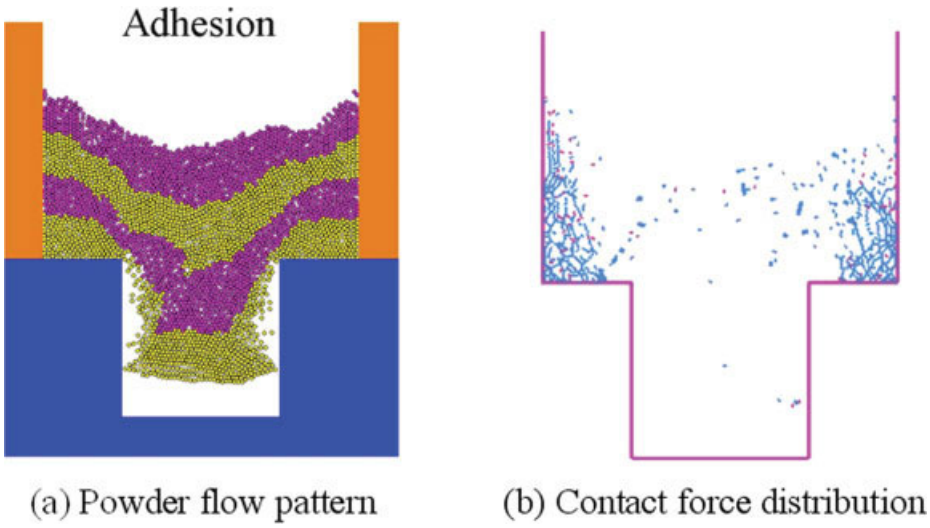

Figure 18. Powder flow pattern (a), and contact force distribution (b), for die filling with adhesion in a vacuum when t = 17 ms.

[Color figure can be viewed in the online issue, which is available at www.interscience.wiley.com.]

than with a noncohesive powder. Furthermore, the dimensionless mass flow rates are much lower for die filling in air than those in a vacuum. This indicates that the presence of air has a more significant effect than adhesion on powder flow, at least for the cases considered here.

Conclusions

In this article, a coupled DEM and CFD method has been used to analyze die filling from a stationary shoe in a vacuum and in air. The influences of particle size, density, size distribution and adhesion on the flow behavior were investigated. It is found that the presence of air has a significant impact on the powder flow behavior, especially for systems with smaller and lighter particles. For the die filling in a vacuum, the dimensionless mass flow rate M^* is found to be constant with a value of 0.58, which is in excellent agreement with the Beverloo constant determined experimentally. The flow characteristics in air depend on the particle size and density. Two distinct regimes have been identified: (1) an air-sensitive regime (for $(\eta^*)^{-2/5}(d_p^*)^{3/5} \leq 19.6$ or Ar $\Phi_\rho \leq 9.56 \times 10^6$) with generally smaller and lighter particles, in which the presence of air has a significant impact on powder flow behavior, and the dimensionless mass flow rate increases as the particle size or density increases, and (2) an air-inert regime (for $(\eta^*)^{-2/5}(d_p^*)^{3/5} > 19.6$ or Ar $\Phi_\rho > 9.56 \times 10^6$), in which the particle size and density are sufficiently large that the effect of air flow becomes negligible, and the dimensionless mass flow rate is essentially identical to that for the die filling in a vacuum. In addition, it was also found

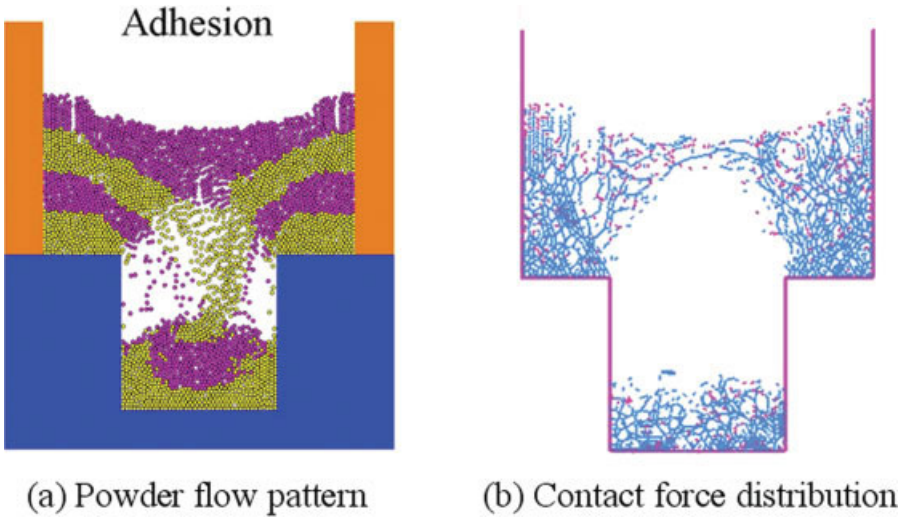

Figure 19. Powder flow pattern (a) and contact force distribution (b) for die filling with adhesion in the presence of air when t = 75 ms.

[Color figure can be viewed in the online issue, which is available at www.interscience.wiley.com.]

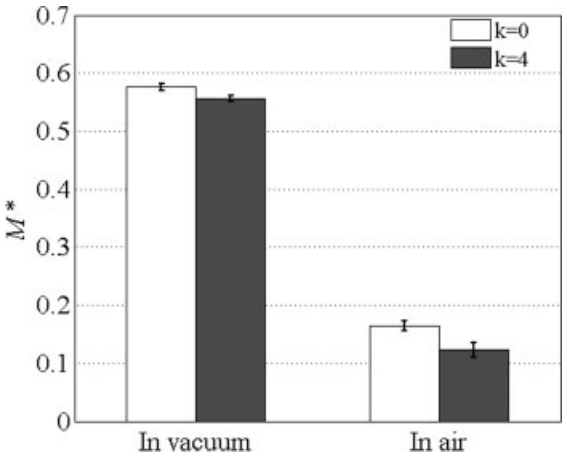

Figure 20. Dimensionless flow rates for different surface energies.

that for die filling in a vacuum, the dimensionless mass flow rate for polydisperse systems is essentially identical to that for monodisperse systems. The presence of air has a more significant impact on the flow of polydisperse powders than monodisperse powders, resulting in a lower dimensionless mass flow rate for polydisperse systems. Finally, it has been demonstrated that the presence of adhesion will slow down the powder flow during die filling in air and in a vacuum. Consequently, a lower dimensionless mass flow rate is obtained for die filling with a cohesive powder when compared to die filling with a noncohesive powder.

Acknowledgments

This work is supported by the Engineering and Physical Sciences Research Council (EPSRC), United Kingdom, through an EPSRC Advanced Research Fellowship awarded to CYW (Grants No: EP/C545230 and EP/C545249).

Literature Cited

1. Coube O, Cocks ACF, Wu CY. Experimental and numerical study of die filling, powder transfer and die compaction. *Powder Metall*. 2005;48(1):68–76.
2. Wu CY, Cocks ACF. Flow behavior of powders during die filling. *Powder Metall*. 2004;47(2):127–136.
3. Xie X, Puri VM. Uniformity of powder die filling using a feed shoe: A review. *Part Sci Technol*. 2006;24(4):411–426.
4. Bocchini GF. Influence of small die width on filling and compacting densities. *Powder Metall*. 1987;30(4):261–266.
5. Haskins JJ, Jandeska WF. Powder flow and die filling studies using computed tomography. Int. Conferance on Powder Metallurgy and Particulate Materials; 31 May-4 June 1999. Las Vegas, NV; 1998:10.77–10.87.
6. Demetry C, Souto FS, Ryden BC, Roy JM. Tactile sensing of density uniformity in powder beds after die filling. *Powder Technol*. 1998;99:119–124.
7. Sawayama T, Seki Y. The effect of filling conditions on die filling. *Adv Powder Metall Part Mater*. 1999;1(2):61–72.
8. Hjortsberg E, Bergquist B. Filling induced density variations in metal powder. *Powder Metall*. 2002;45(2):146–153.
9. Zahrah TF, Rowland R, Gasbarre G Jr. Fluidized fill shoe for uniform die filling. *Key Eng Mater*. 2001;189/191:288–295.
10. Jackson S, Sinka IC, Cocks ACF. The effect of suction during die fill on a rotary tablet press. *Euro J Pharm Biopharm*. 2007;65:253–256.
11. Wu CY, Dihoru L, Cocks ACF. The flow of powder into simple and stepped dies. *Powder Technol*. 2003;134:24–39.
12. Sinka IC, Schneider LCR, Cocks ACF. Measurement of the flow properties of powders with special reference to die fill. *Int J Pharm*. 2004;280:27–38.
13. Schneider LCR, Cocks ACF, Apostolopoulos A. Comparison of filling behaviour of metallic, ceramic, hardmetal and magnetic powders. *Powder Metall*. 2005;48(1):77–84.
14. Schneider LCR, Sinka IC, Cocks ACF. Characterisation of the flow behaviour of pharmaceutical powders using a model die-shoe filling system. *Powder Technol*. 2007;173:59–71.
15. Wu CY, Cocks ACF, Gillia OT. Die filling and powder transfer. *Int J Powder Metall*. 2003;39(4):51–64.
16. Wu CY, Cocks ACF. Numerical and experimental investigations of the flow of powder into a confined space. *Mech Mater*. 2006;38:304–324.
17. Kafui KD, Thornton C, Adams MJ. Discrete particle-continuum fluid modelling of gas-solid fluidised beds. *Chem Eng Sci*. 2002;57:2395–2410.
18. Yang F, Kafui KD, Thornton C, Seville JPK. A DEM study of Geldart Group A particle bed fluidisation behaviour across the regimes. Proceedings of the 12th International Conference on Fluidization; May 13–17, 2007. Vancouver, Canada; 2007.
19. Guo Y, Kafui KD, Thornton C, Wu CY. A numerical study of die filling using a coupled discrete element method and computational fluid dynamics. Proceedings of the European PM; 2007: October 15–17, 2007. Toulouse, France; 2007:317–322.
20. Cundall PA. In M. Satake, J.T. Jenkins, eds. *Micromechanics of Granular Materials*, Amstedam, Elsevier; 1988:113–123.
21. Johnson KL. *Contact Mechanics*. Cambridge: Cambridge University Press; 1985.
22. Johnson KL, Kendall K, Roberts AD. Surface energy and the contact of elastic solids. *Proc R Soc London, Sect A*. 1971;324:301–313.
23. Thornton C. Interparticle sliding in the presence of adhesion. *J Phys D: Appl Phys*. 1991;24:1942–1946.
24. Thornton C. Coefficient of restitution for collinear collisions of elastic-perfectly plastic spheres. *ASME J Appl Mech*. 1997;64(2):383–386.
25. Thornton C, Ning Z. A theoretical model for the stick/bounce behaviour of adhesive, elastic-plastic spheres. *Powder Technol*. 1998;99:154–162.
26. Thornton C, Randall W. In M. Satake, J.T. Jenkins, eds. *Micromechanics of Granular Materials*. Amstedam: Elsevier; 1988:133–142.
27. Thornton C, Yin KK. Impact of elastic spheres with and without adhesion. *Powder Technol*. 1991;65:153–165.
28. Mindlin RD, Deresiewicz H. Elastic spheres in contact under varying oblique forces. *ASME J Appl Mech*. 1953;20:327–344.
29. Tsuji Y, Kawaguchi T, Tanaka T. Discrete particle simulation of two-dimensional fluidized bed. *Powder Technol*. 1993;77:79–87.
30. Seville JPK, Tüzün U, Clift R. *Processing of Particulate Solids*. Blackie Academic and Professional: London; 1997:330–348.
31. Beverloo WA, Leniger HA, Van de Velde J. The flow of granular materials through orifices. *Chem Eng Sci*. 1961;15:260–269.
32. Harmens A. Flow of granular materials through horizontal apertures. *Chem Eng Sci*. 1963;18:297.
33. Brown RL, Richards JC. Kinematics of the flow of dry powders and bulk solids. *Rheol Acta*. 1965;4:153–165.
34. Davidson JF, Nedderman RM. The hour-glass theory of hopper flow. *Trans IChemE*. 1973;51:29–35.
35. Rhodes MJ. *Introduction to particle technology*. Chichester: John Wiley & Sons, Ltd; 1998:213.

Manuscript received Mar. 31, 2008, and revision received Sept. 8, 2008.